Supporting Information:

Oscillatory Active-site Motions Correlate with Kinetic Isotope Effects in Formate Dehydrogenase

Philip Pagano,[1][†] Qi Guo,[1][†] Chethya Ranasinghe,[1] Evan Schroeder,[1] Kevin Robben,[1] Florian Häse,[2] Hepeng Ye,[1] Kyle Wickersham,[1] Alán Aspuru-Guzik,[2,3] Dan T. Major,[4] Lokesh Gakhar,[5] Amnon Kohen[1] and Christopher M. Cheatum[1*]

[1]Department of Chemistry, University of Iowa, Iowa City, IA 52242, United States
[2]Department of Chemistry and Chemical Biology, Harvard University, Cambridge, MA 02138, United States
[3] Senior Fellow, Canadian Institute for Advanced Research (CIFAR), Toronto, Ontario M5G 1Z8, Canada
[4]Chemistry Department, Bar-Ilan University, Ramat Gan 52900, Israel
[5]Protein Crystallography Facility and Department of Biochemistry, University of Iowa, Iowa City, Iowa 52242, United States
[*]To whom correspondence should be addressed; email: christopher-cheatum@uiowa.edu
[†]These two authors contributed equally to this work.

Site-directed mutations – The pET-23a plasmid harboring the gene encoding for FDH was a generous gift from Dr. Nikolaos Labrou of the Agricultural University of Athens. The site-directed mutations were performed following the protocol from Agilent Technologies. The resulting vectors were sequenced by Genomics Division, University of Iowa. For the V123A mutation the forward and reverse primer sequences for mutation were 5'-GTTCTAATGTTGTCTCTG**CGG**CAGAACACGTTCTCATG -3' and 5'-CATGAGAACGTGTTCTG**CCG**CAGAGACAACATTAGAAC -3'. For the V123G mutation the forward and reverse primers sequences for mutations were 5'-CTAATGTTGTCTCTG**GTG**CAGAACACGTTCTC -3' and 5'-GAGAACGTGTTCTG**CAC**CAGAGACAACATTAG-3'. The mutation position is highlighted in bold.

Comparison of mutant FDH to WT FDH

Table S1. Comparison of the steady-state kinetic parameters and azide dissociation constants measured by isothermal titration calorimetry for recombinant, V123A and V123G CbFDHs

	WT	V123A	V123G
k_{cat} (s^{-1})	5.6 ± 0.2	0.11 ± 0.02	0.028 ± 0.003
$K_{M/NAD+}$ (µM)	$30. \pm 2$	$10. \pm 2$	$50. \pm 3$
$k_{cat}/K_{M/NAD+}$ (M^{-1}s^{-1})	$(1.8 \pm 0.1) \times 10^5$	$(1.1 \pm 0.3) \times 10^4$	$(5.6 \pm 0.7) \times 10^3$
$K_{M/formate}$ (mM)	4.0 ± 0.6	1.0 ± 0.3	0.8 ± 0.1
$k_{cat}/K_{M/formate}$ (M^{-1}s^{-1})	$(1.4 \pm 0.2) \times 10^3$	$(1.1 \pm 0.4) \times 10^2$	35 ± 6
$K_{D/azide}$ (nM)	43 ± 5	90 ± 20	40 ± 20

K_D values for azide with the FDH-NAD$^+$ complex were determined using isothermal titration calorimetry (ITC). The ITC experiments are run with all solutions in the same in buffer containing 100 mM phosphate buffer at pH 7.5, consistent with the KIE and 2D IR experimental conditions. We titrate a sample containing 20 µM enzyme and 1mM NAD$^+$ using a titrating solution of 1 mM sodium azide. Figure S1 shows the raw ITC data for the two mutants. The WT result comes from our previous study.
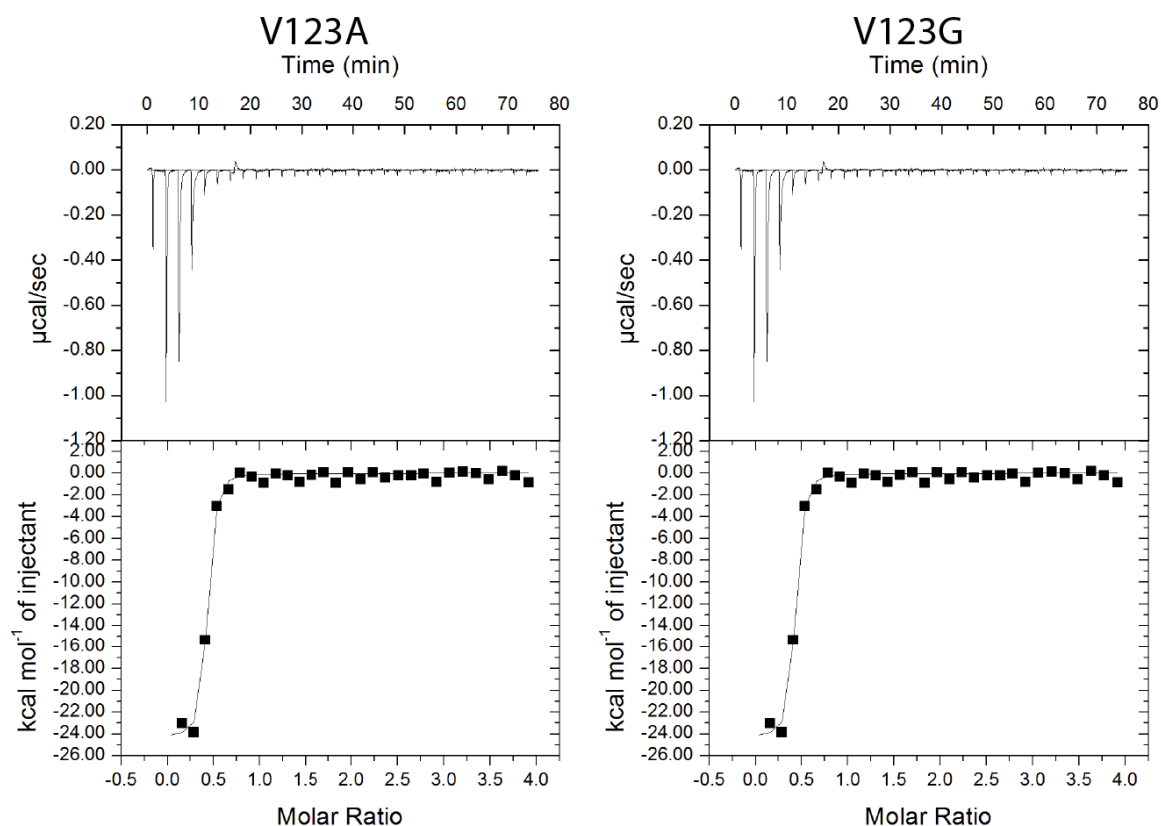
Figure S1 Raw isothermal titration calorimetry data for binding azide to the binary complexes of FDH mutants V123A (left) and V123G (right) each saturated with NAD^+.

Table S2. Observed and Intrinsic KIEs for V123G and V123A mutant.

T, ˚C	V123G			V123A		
	H/T_{obs}	D/T_{obs}	H/T_{int}	H/T_{obs}	D/T_{obs}	H/T_{int}
5	5.08±0.05	2.09±0.03	26±1	4.96±0.03	1.98±0.02	19±1
15	5.6±0.1	2.03±0.03	20±2	5.17±0.02	1.97±0.01	17.5±0.7
25	5.62±0.06	2.00±0.02	17±1	5.54±0.02	1.95±0.01	14.9±0.7
35	5.71±0.01	1.95±0.03	14±1	5.61±0.01	1.94±0.01	14.2±0.3
45	6.44±0.08	1.92±0.01	11±1	6.08±0.02	1.93±0.01	12.5±1.0

Table S3 X-ray Data collection and refinement statistics

	WT (5DN9)	V123A (6D4B)	V123G (6D4C)
Data collection			
Space group	P1 21 1	P1 21 1	P1 21 1
Cell dimensions			
a, b, c (Å)	50.93, 116.62,63.21	51.17, 116.10, 63.09	51.19, 115.90, 65.47
α, β, γ (°)	90.00, 106.90, 90.00	90.00,106.84, 90.00	90.00, 108.56, 90.00
Resolution* (Å)	41.98-1.5(1.58-1.5)	44.94-1.45(1.47-1.45)	45.99-1.45(1.47-1.45)
R_{merge}	0.051 (0.331)	0.052 (0.384)	0.059 (0.637)
$I / \sigma I$	14.8 (3.4)	15.5 (2.5)	13.3 (1.7)
Completeness (%)	95.5 (88.5)	98.7 (91.1)	96.6 (94.4)
Redundancy*	3.1(2.9)	3.5(2.8)	3.7(3.6)
Refinement			
Resolution (Å)	41.98-1.50	44.94-1.45	45.99-1.45
No. reflections	338374	122555	123095
R_{work} / R_{free}	13.8/16.9	15.4/18.0	15.9/18.4
No. atoms			
Protein	5664	5632	5630
Ligand/ion	96	96	96
Water	1084	1055	1148
B-factors	(Ask for input)		
Protein	13.1	10.6	14.4
Ligand/ion	8.3	7.0	10.1
Water	25.37	27.48	23.94
R.m.s. deviations			
Bond lengths (Å)	0.009	0.008	0.009
Bond angles (°)	1.3	1.0	1.0

*Values in parentheses are for highest-resolution shell.
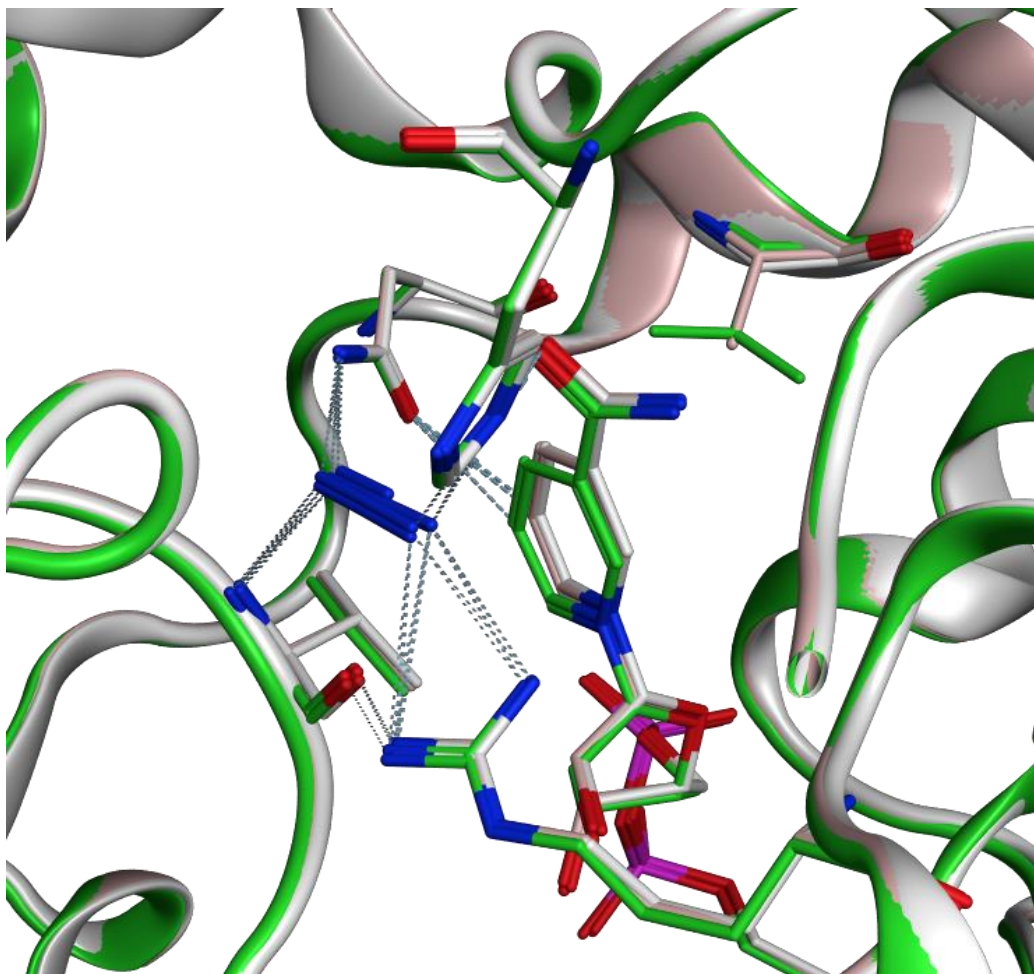
Figure S2 Global superposition of crystal structures 5DN9 (WT in green), 6D4B (V123A in pink) and 6D4C (V123G in white). Note the systematic shift in the position of the nicotinamide ring of NAD^+. Azide also systematically moves in the same direction as the ring, though the shift is considerably smaller than for the ring itself, and all of the H-bonds to the azide in the WT enzyme are preserved in the mutants.

2D IR apparatus and Data Collection

Optical parametric amplification in β-barium borate (BBO) followed by difference frequency generation in $AgGaS_2$ produces ~120 fs mid-IR pulses centered at 2050 cm^{-1} that are separated into pump and a probe pulses. A pulse shaper further separates the pump pulse into two pulses separated in time by τ. A computer-controlled translation stage determines the waiting time, *T*, between the second pump pulse and the probe pulse. For each 2D IR spectrum, a cosine

windowing function apodizes τ to 4 ps. Following upconversion to the visible, a spectrometer disperses the probe spectrum for detection by a 1024-pixel visible array detector, which gives the spectral response along the ω_{probe} axis. The probe spectrum is referenced using an edge-pixel referencing scheme inspired by Feng et al.[1] that significantly reduces the noise associated with shot-to-shot fluctuations of the probe intensity We use a 4-pulse phase cycle and calculate the change in the probe absorbance caused by sequential interactions with the first two pump pulses at each time delay to give a purely absorptive 2D IR signal. Fourier transformation with respect to τ gives the ω_{pump} axis. Waiting times range from 0 to 20 ps, in 50 fs steps.

2D IR sample preparation – The FDH-NAD$^+$-N$_3^-$ ternary complex is prepared in 100 mM phosphate buffer at pH 7.5. The final concentrations for FDH, NAD$^+$ and azide are 1.6, 2 and 1.5 mM, respectively. A 5 μL sample of the ternary complex is placed between CaF$_2$ windows with a 56 μm spacer in a temperature-controlled cell (Harrick Scientific) and incubated at 5 °C for both 2D IR and FT IR measurements.

The day-to-day variations in the 2D IR CLS decay are negligible for consistently prepared samples with nearly the same ratio of protein, cofactor, and inhibitor, even though the signal strength can vary substantially depending on the total concentrations. That is because the lineshape analysis we perform is rather insensitive to variations in intensity associated with concentration changes so long as the azide anion is the minor component meaning that all of it is bound in ternary complexes. Interestingly, however, the observed CLS decays are extremely sensitive to aggregation of the protein. All of the samples exhibit some degree of aggregation over time, especially at the unusually high concentrations required for the 2D IR experiments.

For the WT enzyme, the aggregation is slow enough that a freshly prepared sample will remain

stable in a clean sample cell at 5°C for up to 2 weeks. In contrast, the V123G mutant is

sufficiently less stable that it will show significant signs of aggregation within 2-3 days. As seen

in Figure S3, the CLS decays of the aggregated proteins are marked by a significant increase in

the overall CLS value and a reduction of the oscillatory features in the decay. These changes are

consistent with the increased heterogeneity of the protein that would be expected upon

aggregation.
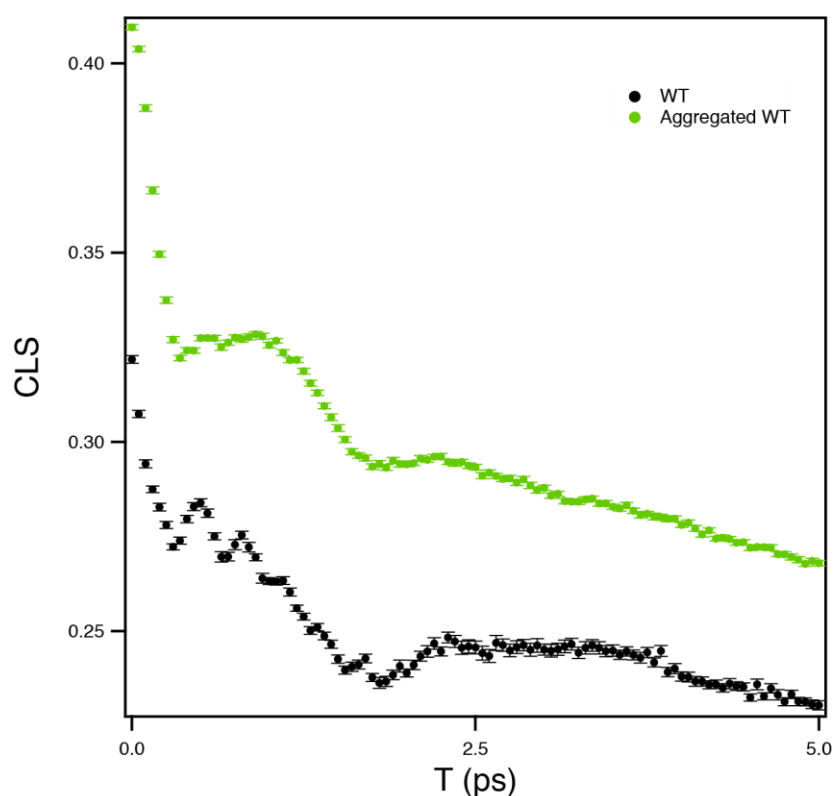
Figure S3 CLS decays for fresh WT and aggregated WT FDH ternary complex samples. The
samples are the same preparation except that the aggregated sample has been stored for longer
than two weeks.

CLS Frequency Analysis We collect CLS data for up to 20 ps (see Figure S4). For the

FFT analysis presented in Figure 3 of the manuscript, we fit the long time decay of the 20 ps data

and subtract that component from the first 5 ps. The longer time component of the subtracted

data will then be exactly zero, allowing us to zero-pad the data to 20 ps for the FFT. This subtraction reduced interference from the large DC component at 0 cm^{-1} but does not alter the amplitude of the 9 cm^{-1} component.

After the FFT of the subtracted data, we fit the first two features, the one centered at zero frequency and the main transition near 9 cm^{-1} to a sum of Gaussians. Table S4 lists the fit parameters for the WT and mutant enzymes

Table S4 Parameters for fitting a sum of Gaussians to the first two transitions in the FFT data of the WT and mutant enzymes shown in Figure 3.

	A_0	FWHM$_0$ (cm^{-1})	A_1	ω_1 (cm^{-1})	FWHM$_1$ (cm^{-1})
WT	0.491 ± 0.005	6.2 ± 0.1	0.507 ± 0.003	8.84 ± 0.03	6.60 ± 0.09
V123A	0.42 ± 0.01	7.0 ± 0.4	0.636 ± 0.004	9.0 ± 0.1	10.6 ± 0.3
V123G	0.204 ± 0.007	4.5 ± 0.2	0.791 ± 0.003	9.18 ± 0.02	10.03 ± 0.09
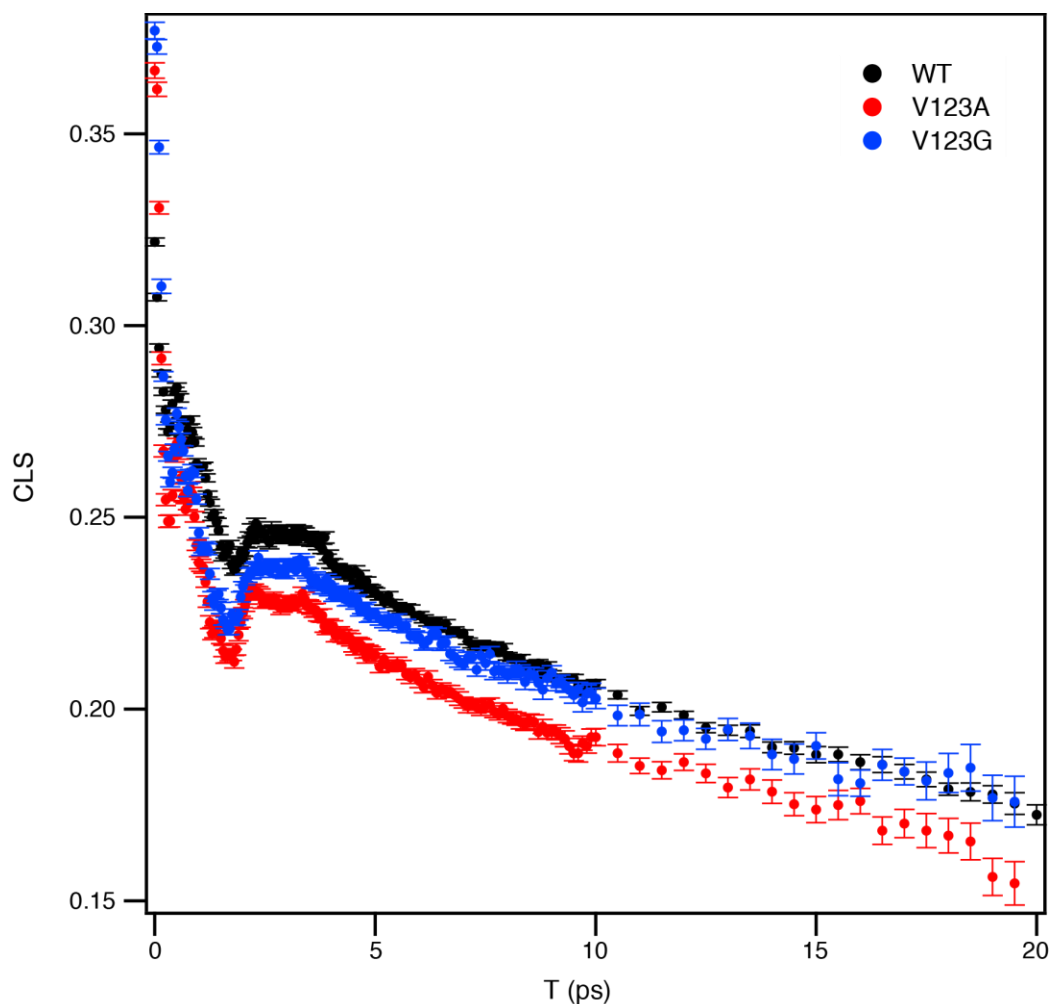
Figure S4 CLS decays plotted as a function of waiting time (T) for azide ternary complexes with NAD^+ in WT FDH (black), V123A (red), and V123G (blue). Data are measured to a waiting time of 20 ps at which point the thermal response due to heating of the solution becomes comparable in magnitude to the remaining response due to the very small number of vibrationally excited molecules remaining in the system causing the correlation to drop precipitously at longer waiting times.

Azide force correlation calculations

Methods

Initial structures for the presented MD studies on the wild type were constructed from the crystal structure of holo CbFDH (PDB: 5DN9). Mutant structures were prepared based on the crystal structures 5DN9, 6D4B, and 6D4C. Protonation states of all amino acids in these three complexes were determined from the H++ protonation server for pH 7.[3] All complexes were solvated in cuboidal periodic boxes with at least 15 Å distance between the complexes and the box boundaries. Explicit water molecules were parametrized as three-point charges with the

TIP3PF water model.[4] Amino acids were modeled with the Amber ff14 force field.[5] Force field parameters for the azide and NAD+ were obtained from the generalized amber force field (GAFF).[6, 7] For each generated system the total charge was neutralized by adding sodium ions. Long-range electrostatic interactions are computed with the Particle-Mesh Ewald method.[8]

After an energy minimization of the three complexes based on 5000 iterations of steepest descent followed by 5000 iterations of conjugate gradient the systems were equilibrated gradually in the NPT ensemble to a target temperature of 300 K and a target pressure of 1 bar. The equilibrations were run for a total of 100 ns. Temperature was controlled with the extended Nose-Hoover thermostat,[9] and pressure was controlled via isotropic position scaling. The equations of motion were integrated in a leap-frog integration scheme with a time step of 2 fs and SHAKE constraints bonds involving hydrogen. All simulations were run in the Amber software package, version 15 [10].

Subsequent to the equilibration we continued the MD simulations by 100 ps with integration steps of 1 fs and no constraints on any of the bonds. During this production run, we recorded atom positions and forces between atoms every 4 fs. All other simulation parameters are identical to the equilibration runs.

Results

Force correlation function (FCF) curves were computed from MD simulations following the methodology previously described.[11] In this approach, the interaction potential between the azide and its environment is expanded in terms of normal coordinates. The frequency shift can then be expressed in terms of the mass-weighted intermolecular force on the azide projected onto the normal coordinate of interest, i.e. the antisymmetric stretch mode. The correction on the frequency can be calculated via perturbation theory

$$\delta\omega(t) = \frac{3}{2\omega_0}\sqrt{\frac{\Delta}{\hbar\mu}}F(t)$$

where μ denotes the reduced mass associated with the antisymmetric stretch, Δ denotes the anharmonic shift of the antisymmetric vibration ($\Delta = 26\ cm^{-1}$) and $\omega_0 = 2050\ cm^{-1}$ is the gas-phase vibrational frequency.[12] With this frequency shift we compute the FFCF to be linearly proportional to the FCF.

In particular, we focus on the computation of the FCF in the IR active antisymmetric stretch mode of the azide. FCF curves obtained from the MD simulations are presented in the main text in Figure 5. Figure S5 depicts the Fourier transform of the FCF traces. Note that although the overall amplitude of the spectral density of the FCF is smaller for the mutant variants than for the WT enzyme, the relative size of the peak at 10 cm^{-1} is slightly larger for the V123A variant than the WT. This effect is smaller than what is seen experimentally, and it is clear that the experimental and computational results do not exhibit quantitative agreement. Nevertheless, the trend is consistent, though it does breakdown for the V123G variant where the changes to the FCF spectral density are not consistent with the experimental results even qualitatively.

We then compute the distances between the C4 position of the nicotinamide ring and the central nitrogen in the azide (DAD). Figure 6 in the main text displays the distributions of the DAD for the three complexes computed over the entire range of the production runs. We observe a general trend for larger distances along with larger fluctuations in the distance with increasing active site space.
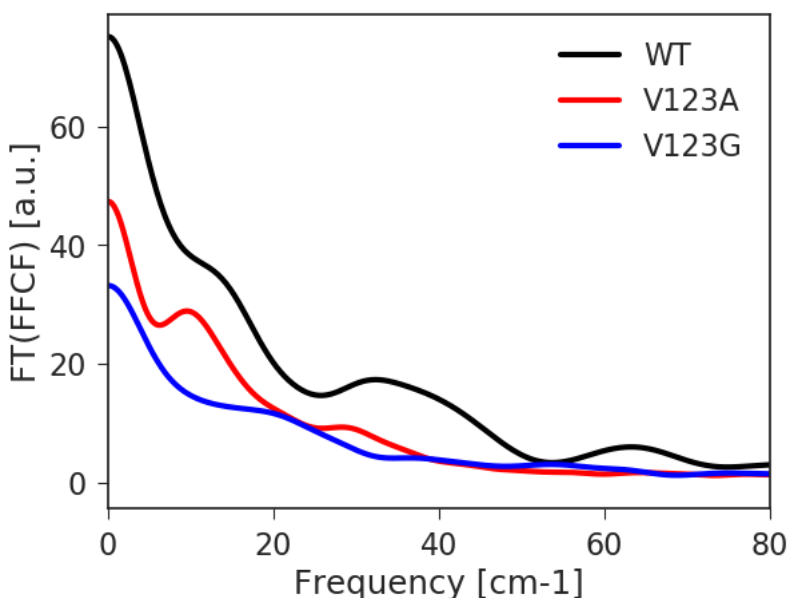
Figure S5 Fourier transforms of Azide's FCF obtained simulations of the azide-FDH.

QM/MM Free energy calculations for hydride transfer.

The crystal structure of holo-CbFDH (PDB 5DN9) was used to construct the initial systems for the present study.[13] The setup and the MD simulations of all systems were carried out based on procedures similar to those employed in previous studies.[13, 14] Briefly, the protonation states of all polar amino acid residue side chains were adjusted to pH 7, and the protonation states of the His residues were determined so as to match the hydrogen bonding patterns in the nearest environment. The HBUILD facility in the program CHARMM[15, 16] was applied to add hydrogen atoms. Periodic boundary conditions were employed to solvate the Michaelis complex using a pre-equilibrated cubic water box (~97 Å × ~97 Å × ~97 Å). Two sodium ions were added to the WT system to neutralize the overall negative charge. The energy minimized WT structure has a RMSD of 0.180 Å relative to the crystal structure. The V123A and V123G mutants were generated in-silico by point-mutations to the WT structure, as the mutant crystal structures were not available at the outset of this study. The setup protocol was

identical to that of the WT enzyme. Comparison of the energy minimized mutant systems with their respective crystal structures solved in the current study, reveals increases in the small root-mean-square deviations (RMSD) between the experimental and computational systems of 0.184 Å and 0.219 Å, suggesting that in-silico point mutation is a reasonable protocol for the current study

The potential energy surface in the current study is described by a hybrid QM/MM Hamiltonian,[17] where the QM region is treated by a modified AM1[18] semiempirical Hamiltonian, denoted AM1-SRP (specific reaction parameters).[14,19] The QM region includes the fragments NADH and CO_2, which are proximal to the reaction center, whereas the MM region contains the remaining ligand atoms, the entire protein, water molecules and sodium ions. The water molecules were represented by the three-point charge TIP3P model.[20] The QM/MM interactions were treated using electrostatic embedding. A detailed QM/MM partitioning scheme and a thorough description of the development of the AM1-SRP Hamiltonian for FDH is provided elsewhere.[14] In modeling the MM region, we used the all-atom CHARMM22 force field.[21]

Long-range electrostatic interactions were treated with the Ewald summation technique ($96 \times 96 \times 96$ FFT grid and $\kappa = 0.340$ Å^{-1}).[22] The WT and mutant systems were fully minimized, and heated up gradually to 298 K for 25 ps using molecular dynamics (MD) simulations. All systems were equilibrated at that temperature for 1 ns at the MM level of theory. Each system was thereafter re-equilibrated using the QM(AM1-SRP)/MM potential over the course of 200 ps. All equilibrations and subsequent simulations were conducted with the isothermal-isobaric (*NPT*) ensemble at 1 atm and at the target experimental temperature. The pressure and temperature were controlled by the extended constant pressure/temperature (CPT) method[23, 24] and the Hoover thermostat,[25] respectively. The leapfrog integration scheme[26] was used to

propagate the equations of motion, and the SHAKE algorithm[27] was applied to constrain all MM bonds involving hydrogen atoms, allowing a time step of 1 fs. During the equilibration, several nuclear Overhauser effect (NOE) restraints were imposed on key hydrogen bond interactions between the ligands and the surrounding residues, and removed 200 ps before moving on to the production phase. All enzyme simulations used a development version of the CHARMM program.[15, 16] Complementary details of the MD simulations are available in our earlier work.[14]

The umbrella sampling (US) technique[28] was used to determine the classical-mechanical potential of mean force (CM-PMF) for the hydride transfer reaction. The reaction coordinate was defined as the antisymmetric reactive stretch coordinate, ζ_{asym}, namely the difference between the lengths of the breaking C–H and forming H–C4N bonds. A total of 14 individual US MD simulations ("windows") were performed along discrete, evenly spaced values of ζ_{asym} from -1.75 to 1.5 Å. Each window was subject to an appropriate harmonic restraint, which keeps ζ_{asym} in the desired region, and an umbrella potential (roughly the negative of the PMF) as a function of ζ_{asym}. The cumulative simulation time per window was 375-400 ps. The statistics for all coordinates were sorted into bins of width 0.01 Å. CM-PMF curves and surfaces were computed using a multidimensional version of the weighted histogram analysis method (WHAM).[29] Quantum mechanical corrections to the CM PMFs were obtained by path-integral simulations as described in our earlier works.[14, 30-32]

To obtain DAD distribution functions we collected the DAD from reactant state (RS) and transition state (TS) trajectories. In the case of the RS, these were unbiased MD simulations of the Michaelis complex, while the TS was constrained to the reaction coordinate value corresponding to the maximum of the PMF, using the SHAKE algorithm,[27] as implemented in the RCON BDIS command in CHARMM.

Computational Results

The experimentally observed k_{cat} rates may be translated into phenomenological free energy barriers, $\Delta G^{\ddagger}$, via Eyring's equation. Consequently, the experimental $\Delta G^{\ddagger}$ values for WT, V123A, and V123G are 16.4, 18.8, and 19.6 kcal/mol, respectively. The corresponding simulated multiscale free energy barriers for WT, V123A, and V123G reproduce the experimental trends reasonably well with $\Delta G^{\ddagger}$ values of 13.5, 16.1, and 19.2 kcal/mol, respectively. We note that the theoretical values obtained in Table S5 are from classical PMF free energy simulations (Figure S6) and path-integral nuclear quantum corrections. We ascribe the higher free energy barriers in the mutant enzymes to a greater reorganization cost as the enzyme moves from the RS to the TS, similar to what was found for analogous mutants in E. Coli dihydrofolate reductase.[33] Inspection of the shape of the PMF curve in the RS region of the WT enzyme (Figure S6) reveals that formate might bind in two states, corresponding to the two possible orientations of the formate hydrogen atom relative to the C4 atom of NAD^+. In the mutant enzymes, these states are not distinguishable, as there is more room for the formate-NAD^+ reactive complex to move around. Additionally, the RS region is shallower as the size of the amino acid at position 123 is reduced.

To obtain better understanding of the effect of the V123 mutation on the DAD, we plot the DAD distribution obtained from multiscale MD simulations for the RS and TS (Figure S7). In the RS the DAD distribution is clearly wider and shifted to longer DADs for the mutant enzymes, and this behavior is most noticeable for the V123G mutant. Additionally, the mutant's RS distributions appear wider than that of the WT enzyme. These DAD distributions reflect the increasingly greater active site space available to the reactive complex as a result of the V123

mutation. On the other, in the TS the DAD distributions are very similar, although a slight shift to greater DADs is observed for the mutants.

Table S5. Free energies of activation, $\Delta G^{\ddagger}$, (kcal/mol) calculated from classical (CM) and quantum mechanical (QM) potentials of mean force for the hydride transfer from formate to NAD^+ in WT (blue), V123A (red) and V123G (green) variants of CbFDH
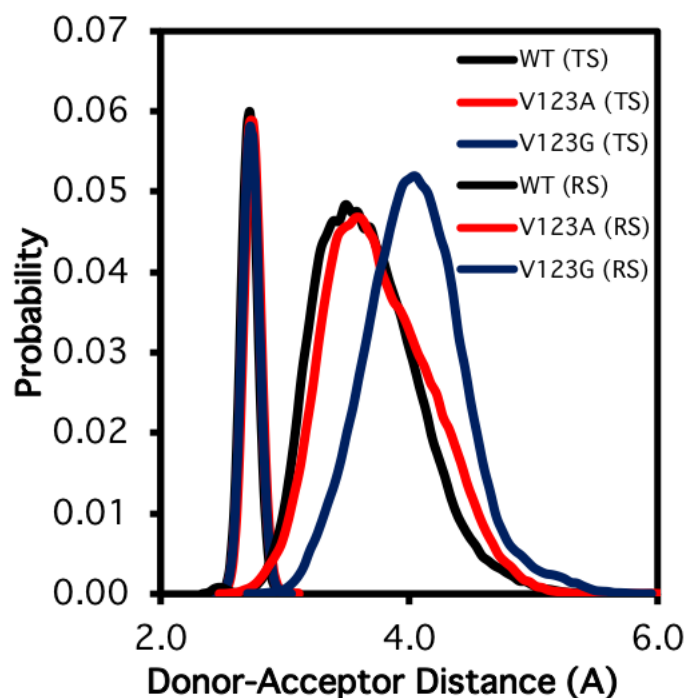
	$\Delta G^{\ddagger}_{CM}$	$\Delta G^{\ddagger}_{QM}$	$\Delta G^{\ddagger}$ (Exp)[a]
WT	15.7	13.5	16.4
V123A	18.5	16.1	18.8
V123G	21.9	19.2	19.6

[a] Obtained from Eyring's equation and the experimental k_{cat}, $\Delta G^{\ddagger}=-RT\cdot\ln(k_{cat}\,h/k_{B}T)$.
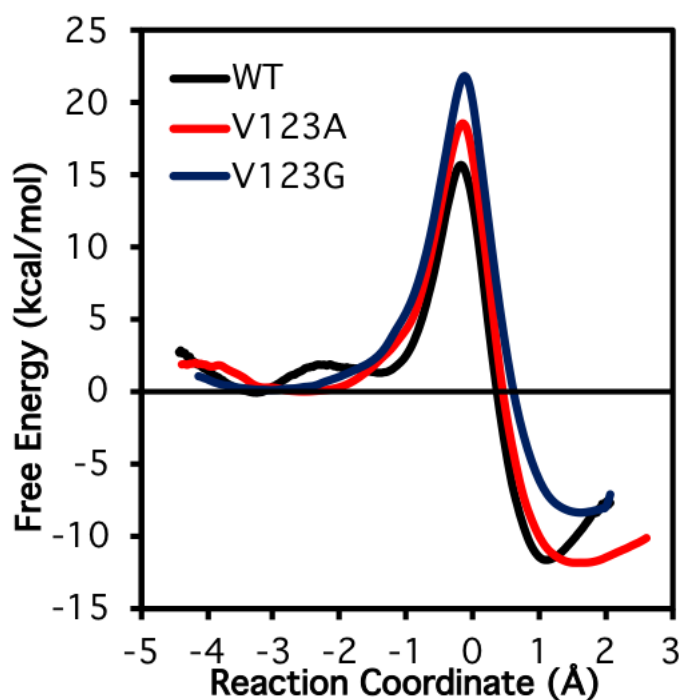
Figure S6 Classical free energy profiles for the hydride transfer from formate to NAD^+ in WT (black), V123A (red) and V123G (blue) variants of CbFDH.

Figure S7 Donor-Acceptor distance distribution functions obtained from classical multiscale MD simulations of the RS, which are all at longer DAD, and TS, which are clustered tightly at short DAD, for WT, V123A, and V123G forms of CbFDH

References:

1.   Feng, Y.; Vinogradov, I.; Ge, N.-H., General noise suppression scheme with reference detection in heterodyne nonlinear spectroscopy. *Optics Express* **2017,** *25* (21), 26262-26279.

2.   Pagano, P.; Guo, Q.; Kohen, A.; Cheatum, C. M., Oscillatory Enzyme Dynamics Revealed by Two-Dimensional Infrared Spectroscopy. *J Phys Chem Lett* **2016**, 2507-2511.

3.   Anandakrishnan, R.; Aguilar, B.; Onufriev, A. V., H++ 3.0: automating pK prediction and the prepatration of biomolecular structures of atomistic molecular modeling and simulation. *Nucleic Acid Research* **2012,** *40*, 537-541.

4.   Price, D. J.; Brooks, C. L. A., A modified TIP3P water potential for simulation with Ewald summation. *Journal of Chemical Physics* **2004,** *121*, 10096-10103.

5.   Maier, J. A.; Martinez, C.; Kasavajhala, K.; Wickstrom, L.; Hause, K. E.; Simmerling, C., ff14SB: improving the accuracy of protein side chain and backbone parameters from ff99SB. *Journal of Chemical Theory and Computation* **2015,** *11*, 3696-3713.

6.   Wang, J.; Wang, W.; Kollman, P. A.; Case, D. A., Automatic atom type and bond type perception in molecular mechanical calculations. *Journal of Molecular Graphics and Modelling* **2006,** *25*, 247260.

7.   Wang, J.; Wolf, R. M.; Caldwell, J. W.; Kollman, P. A.; Case, D. A., Development and testing of a general AMBER force field. *Journal of Computational Chemistry* **2004,** *25*, 1157-1174.

8.   Essman, U.; Perera, L.; Berkowitz, M. L.; Darden, T.; Lee, H.; Pederson, L., A smooth particle mesh Ewald method. *Journal of Chemical Physics* **1995,** *103*, 8577-8593.

9.   Omelyan, I.; Kovalenko, A., Generalized canonical-isokinetic ensemble: Speeding up multiscale molecular dynamics and coupling with 3d molecular theory of solvation. *Molecular Simulation* **2013,** *39*, 25-48.

10.   Case, D. A.; Berryman, J. T.; Betz, R. M.; Cerutti, D. S.; Cheatham III, T. E.; Darden, T. A.; Duke, R. E.; Giese, T. J.; Gohlke, H.; Goetz, A. W.; Homeyer, N.; Izadi, S.; Janowski, P.; Kaus, H.; Kovalenko, A.; Lee, T. S.; LeGrand, S.; Li, P., Luchko; T., L., E.; Madej, B.; Merz, K. M.; Monard, G.; Needham, P.; Nguyen, H.; Nguyen, H. T.; Omelyan, I.; Onufriev, A. V.; Roe, D. R.; Roitberg, A.; Salomon-Ferrer, R.; Simmerling, C. L.; Smith, W.; Swails, J.; Walker, R. C.; Wang, J.; Wolf, R. M.; Wu, X.; York, D. M.; Kollman, P. A., AMBER 2015, University of California, San Francisco. **2015**.

11.   Hamm, P.; Zanni, M. T., *Concepts and Methods of 2D Infrared Spectroscopy*. Cambridge University Press: New York, NY, 2011.

12.   Gai, X. S.; Coutifaris, B. A.; Brewer, S. H.; Fenlon, E. E., A direct comparison of axide and nitrile vibrational probes. *Physical Chemistry Chemical Physics* **2011,** *13*, 5926-5930.

13.   Guo, Q.; Gakhar, L.; Wickersham, K.; Francis, K.; Vardi-Kilshtain, A.; Major, D. T.; Cheatum, C. M.; Kohen, A., Structural and Kinetic Studies of Formate Dehydrogenase from Candida boidinii. *Biochemistry* **2016,** *55*, 2760-2771.

14.   Vardi-Kilshtain, A.; Major, D. T.; Kohen, A.; Engel, H.; Doron, D., Hybrid Quantum and Classical Simulations of the Formate Dehydrogenase Catalyzed Hydride Transfer Reaction on an Accurate Semiempirical Potential Energy Surface. *J. Chem. Theory Comput.* **2012,** *8* (11), 4786-4796.

15.   Brooks, B. R.; Bruccoleri, R. E.; Olafson, B. D.; States, D. J.; Swaminathan, S.; Karplus, M., CHARMM: A program for macromolecular energy, minimization, and dynamics calculations. *J. Comput. Chem.* **1983,** *4* (2), 187-217.

16.   Brooks, B. R.; Brooks, C. L.; Mackerell, A. D.; Nilsson, L.; Petrella, R. J.; Roux, B.; Won, Y.; Archontis, G.; Bartels, C.; Boresch, S.; Caflisch, A.; Caves, L.; Cui, Q.; Dinner, A. R.; Feig, M.; Fischer, S.; Gao, J.; Hodoscek, M.; Im, W.; Kuczera, K.; Lazaridis, T.; Ma, J.; Ovchinnikov, V.; Paci, E.; Pastor, R. W.; Post, C. B.; Pu, J. Z.; Schaefer, M.; Tidor, B.; Venable, R. M.; Woodcock, H. L.; Wu, X.; Yang, W.; York, D. M.; Karplus, M., CHARMM: The biomolecular simulation program. *J. Comput. Chem.* **2009,** *30* (10), 1545-1614.

17.   Warshel, A.; Levitt, M., Theoretical studies of enzymic reactions: Dielectric, electrostatic and steric stabilization of the carbonium ion in the reaction of lysozyme. *J. Mol. Biol.* **1976,** *103* (2), 227-249.

18.   Dewar, M. J. S.; Zoebisch, E. G.; Healy, E. F.; Stewart, J. J. P., Development and use of quantum mechanical molecular models. 76. AM1: a new general purpose quantum mechanical molecular model. *J. Am. Chem. Soc.* **1985,** *107* (13), 3902-3909.

19.   Rossi, I.; Truhlar, D. G., Parameterization of NDDO wavefunctions using genetic algorithms. An evolutionary approach to parameterizing potential energy surfaces and direct dynamics calculations for organic reactions. *Chem. Phys. Lett.* **1995,** *233* (3), 231-236.

20.   Jorgensen, W. L.; Chandrasekhar, J.; Madura, J. D.; Impey, R. W.; Klein, M. L., Comparison of simple potential functions for simulating liquid water. *J. Chem. Phys.* **1983,** *79* (2), 926-935.

21.   MacKerell, A. D.; Bashford, D.; Bellott, M.; Dunbrack, R. L.; Evanseck, J. D.; Field, M. J.; Fischer, S.; Gao, J.; Guo, H.; Ha, S.; Joseph-McCarthy, D.; Kuchnir, L.; Kuczera, K.; Lau, F. T. K.; Mattos, C.; Michnick, S.; Ngo, T.; Nguyen, D. T.; Prodhom, B.; Reiher, W. E.; Roux, B.; Schlenkrich, M.; Smith, J. C.; Stote, R.; Straub, J.; Watanabe, M.; Wiórkiewicz-Kuczera, J.; Yin,

D.; Karplus, M., All-Atom Empirical Potential for Molecular Modeling and Dynamics Studies of Proteins. *J. Phys. Chem. B* **1998,** *102* (18), 3586-3616.

22.   Nam, K.; Gao, J.; York, D. M., An Efficient Linear-Scaling Ewald Method for Long-Range Electrostatic Interactions in Combined QM/MM Calculations. *J. Chem. Theory Comput.* **2005,** *1* (1), 2-13.

23.   Andersen, H. C., Molecular dynamics simulations at constant pressure and/or temperature. *J. Chem. Phys.* **1980,** *72* (4), 2384-2393.

24.   Feller, S. E.; Zhang, Y.; Pastor, R. W.; Brooks, B. R., Constant pressure molecular dynamics simulation: The Langevin piston method. *J. Chem. Phys.* **1995,** *103*, 4613-4621.

25.   Hoover, W. G., Canonical dynamics: Equilibrium phase-space distributions. *Phys Rev. A* **1985,** *31* (3), 1695-1697.

26.   Hockney, R. W., Potential calculation and some applications. *Methods Comput. Phys.* **1970,** *9*, 135-211.

27.   Ryckaert, J.-P.; Ciccotti, G.; Berendsen, H. J. C., Numerical integration of the cartesian equations of motion of a system with constraints: molecular dynamics of n-alkanes. *J. Comput. Phys.* **1977,** *23* (3), 327-341.

28.   Torrie, G. M.; Valleau, J. P., Nonphysical sampling distributions in Monte Carlo free-energy estimation: Umbrella sampling. *J. Comput. Phys.* **1977,** *23* (2), 187-199.

29.   Kumar, S.; Rosenberg, J. M.; Bouzida, D.; Swendsen, R. H.; Kollman, P. A., THE weighted histogram analysis method for free-energy calculations on biomolecules. I. The method. *J. Comput. Chem.* **1992,** *13* (8), 1011-1021.

30.   Major, D. T.; Gao, J. L., Implementation of the bisection sampling method in path integral simulations. *Journal of Molecular Graphics and Modelling* **2005,** *24* (2), 121-127.

31.   Major, D. T.; Garcia-Viloca, M.; Gao, J. L., Path integral simulations of proton transfer reactions in aqueous solution using combined QM/MM potentials. *Journal of Chemical Theory and Computation* **2006,** *2* (2), 236-245.

32.   Major, D. T.; Gao, J. L., An integrated path integral and free-energy perturbation-umbrella sampling method for computing kinetic isotope effects of chemical reactions in solution and in enzymes. *Journal of Chemical Theory and Computation* **2007,** *3* (3), 949-960.

33.   Doron, D.; Stojkovic, V.; Gakhar, L.; Vardi-Kilshtain, A.; Kohen, A.; Major, D. T., Free Energy Simulations of Active-Site Mutants of Dihydrofolate Reductase. *Journal of Physical Chemistry B* **2015,** *119* (3), 906-916.